PHYSICAL REVIEW A **75**, 020703(R) (2007)

Gas-solid difference in charge-changing cross sections for bare and H-like nickel ions at 200 MeV/u

H. Ogawa,[1] H. Geissel,[2,3] A. Fettouhi,[2,3] S. Fritzsche,[4] M. Portillo,[5] C. Scheidenberger,[2] V. P. Shevelko,[6] A. Surzhykov,[7] H. Weick,[2] F. Becker,[2] D. Boutin,[2] B. Kindler,[2] R. K. Knöbel,[2,3] J. Kurcewicz,[8] W. Kurcewicz,[8] Yu. A. Litvinov,[2,3] B. Lommel,[2] G. Münzenberg,[2] W. R. Plaß,[3] N. Sakamoto,[1] J. Stadlmann,[2] H. Tsuchida,[1] M. Winkler,[2] and N. Yao[2]

[1]*Department of Physics, Nara Women's University, Nara 630-8506, Japan*

[2]*Gesellschaft für Schwerionenforschung GSI, Planckstraße 1, 64291 Darmstadt, Germany*

[3]*II. Physikalisches Institut, Justus-Liebig Universität Gießen, Heinrich-Buff-Ring 14, D-35392 Gießen, Germany*

[4]*Institut für Physik, University of Kassel, Heinrich-Plett-Strasse 40, D-34132 Kassel, Germany*

[5]*National Superconducting Cyclotron Laboratory, Michigan State University, East Lansing, Michigan 48824, USA*

[6]*P.N. Lebedev Physical Institute, Leninski prospect 53, 119991 Moscow, Russia*

[7]*Max-Planck-Institut für Kernphysik, Saupfercheckweg 1, D-69117 Heidelberg, Germany*

[8]*Institute of Experimental Physics, Warsaw University, PL-00681 Warsaw, Poland*

(Received 7 October 2005; published 26 February 2007)

It is well known that the density of the target can have a crucial impact on charge-changing collisions of partially ionized heavy ions. However, the basic understanding of this experimental observation is hampered by the difficulty in knowing the charge-state evolution of projectiles inside solids. Therefore, the present experiments with 200 MeV/u bare and H-like nickel ions were performed to study charge-changing cross sections in different monatomic and compound gases and solids. The experimental results clearly demonstrate that the electron-loss cross sections in solids increase by about 40% compared to gases. The results support the Bohr-Lindhard model which predicts this gas-solid difference originating from enhanced ionization of excited ions. The experimental results are compared with recent theoretical estimates.

DOI: 10.1103/PhysRevA.75.020703 PACS number(s): 34.70.+e

The density of target atoms can strongly affect the charge-state distribution of partially ionized heavy ions. This has been discovered in pioneer measurements with fission fragments [1] and is still an unsolved problem which continuously motivates new experimental and theoretical approaches [2–8]. The first theoretical model for this phenomenon was postulated by Bohr and Lindhard [9] who explained the observed density effect by different collision rates inside the media. As a consequence, the higher charge states of heavy ions in solids should cause an enhanced stopping power. However, the early experiments could not confirm this feature due to restricted projectile-energy combinations. Therefore, Betz and Grodzins [10] proposed a new model assuming that the observed charge-state difference is mainly caused by the deexcitation of projectiles via Auger cascades after emerging from a solid medium. Only much later, with the invention of new powerful accelerator facilities, was the density effect discovered in the stopping power of heavy ions [3,11]. Other stopping-power experiments, under preequilibrium target conditions, have also demonstrated the crucial and complex role of the charge-state evolution [12]. The dependence on chemical binding and physical state effects is reviewed in Ref. [13].

However, a proper understanding of this basic atomic collision problem has not been achieved yet. Quantitative comparisons of the experimental results from charge-state distribution and stopping-power measurements reveal that, in general, the observed enhancement of the mean charge after passage through dense media is larger than expected from the corresponding observed increase in the stopping power. On the other hand, the predicted number of missing Auger electrons to balance the difference has not been found either [5,14,15]. This situation motivated our present effort using the unique experimental conditions provided by relativistic heavy projectiles.

Our measurements were performed with the heavy-ion synchrotron SIS [16] and the magnetic spectrometer FRS at GSI [17]. Projectiles of 200 MeV/u Ni^{27+} were selected and focused on monatomic and compound gases and solids placed at the central focal plane of the FRS. The following target materials were used for solids and gases: (i) polypropylene $(C_3H_6)_n$, carbon, aluminum, and titanium in the thickness range of 0.5–45 mg/cm^2, and (ii) ethylene C_2H_4, nitrogen, and neon in the thickness range of 1–68 mg/cm^2. The gases were confined in a window-sealed gas cell operated in flow mode with a precise pressure controlling system. The windows consisted of 6 μm $(C_3H_6)_n$ foils with 5 mm diameter. The cell length along the beam path was 312 mm. The gas pressure was variable up to 2000 mbar and was kept constant at a selected pressure within an accuracy of 0.1% by an automatically adjusted gas flow. Measurements of the window deformation as a function of the gas pressure revealed a negligible influence on the actual length of the gas column.

Details of the experimental setup will be presented in Ref. [18]. Except for the gas-cell apparatus, the experimental setup is similar to that employed in our previous atomic collision studies at the FRS [19]. The different charge states of nickel ions, transmitted through the targets, were spatially separated by the third magnetic-dipole stage of the FRS and measured with a position-sensitive two-dimensional multiwire proportional counter (MWPC) followed by a plastic scintillator. The latter detector was required for MWPC efficiency corrections. The intensity of the projectiles was only a

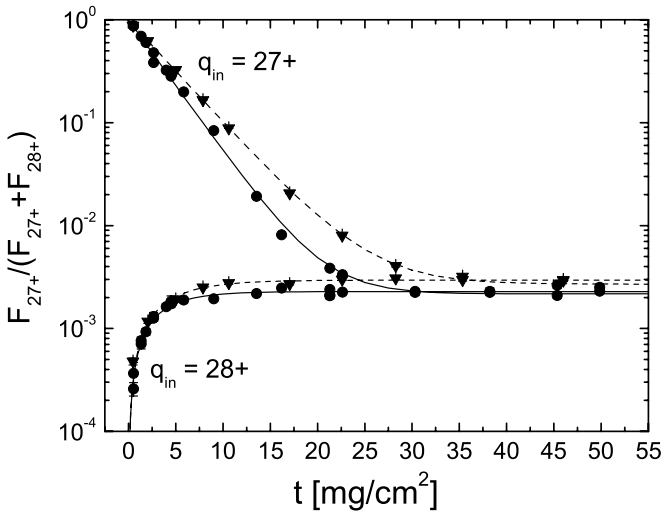

FIG. 1. Measured charge-state fractions for 200 MeV/u Ni^{27+} ions emerging from targets of polypropylene [$(C_3H_6)_n$, solid], indicated by triangles, and ethylene (C_2H_4, gaseous), represented by circles. The data are shown as a function of the target thickness for incoming beams of Ni^{27+} (q_{in}=27+) and of Ni^{28+} (q_{in}=28+). The solid and dashed curves represent the weighted least-squares fits applying Eqs. (1) and (2) for $(C_3H_6)_n$ and C_2H_4. Where error bars are not visible, they are smaller than the data points.

few thousand per second; thus practically no radiation damage was induced in the target media and detectors. Mainly bare and H-like ions contribute to the measured distributions due to the chosen kinetic energy of the projectiles. The equilibrium fraction of He-like ions was smaller than 3×10^{-4} for all targets. Furthermore, the ratio of He-like to H-like ions was less than 0.04. Therefore, the charge-state evolution of the incident H-like ions can be described with good accuracy by considering only the bare and H-like components. Thus we can apply the two-charge-state model for the analysis of the measured fraction of H-like Ni^{27+} ions characterized by the equation

$$F_{27+}(t)=\frac{\sigma_C}{\sigma_C+\sigma_L}+\frac{\sigma_L}{\sigma_C+\sigma_L}\exp\{-N_t(\sigma_C+\sigma_L)t\}, \quad (1)$$

where σ_L and σ_C denote the cross sections for electron loss of H-like ions and capture of bare ions, respectively. N_t and t represent the number of target atoms (molecules) per unit mass and the foil thickness in units of mass per unit area.

An analogous analysis was also performed for the experimental charge-state fractions created in electron-capture collisions of incident bare ions:

$$F_{27+}(t)=\frac{\sigma_C}{\sigma_C+\sigma_L}[1-\exp\{-N_t(\sigma_C+\sigma_L)t\}]. \quad (2)$$

The σ_L and σ_C values were determined by least-squares fits to the measured $F_{27+}(t)$ fractions applying Eqs. (1) or (2).

A representative and important example of the experimental charge-state fractions is presented in Fig. 1 for the polypropylene and ethylene targets. The upper and lower parts of the figure correspond to the charge-state evolution of incident H-like (q_{in}=27+) and bare (q_{in}=28+) Ni ions, respectively. The charge-state distribution after penetrating the gas cell was measured at each gas pressure for both incident H-like and bare projectiles. With these data and the cross sections separately measured in polypropylene foils, the window correction for the gas measurements was derived according to the matrix formalism [20]. About 76% of the H-like ions remained in the incident charge state after traveling through the two windows of the evacuated gas cell. The window measurements were repeated before and after each series of gas measurements. The agreement of H-like fractions demonstrates that there was no significant deterioration of the $(C_3H_6)_n$ foils due to the beam irradiation.

An independent check for these results was performed with $(C_3H_6)_n$ foils of the same thickness as used for the windows but mounted on the target ladder with the other solid targets. The excellent agreement of the two measurements confirms that no significant systematic error, due to the window setup, masks the results for gases and solids.

TABLE I. Electron-loss σ_L and -capture σ_C cross sections for 200 MeV/u Ni ions colliding with gaseous and solid targets. The label "expt." indicates experimental data of this work. The theoretical electron-loss cross sections indicated by DIRAC and LOSS were calculated with the corresponding codes. The total capture cross sections (NRC+REC) were calculated with the DIRAC (REC) and the CAPTURE (NRC) codes.

Target	Phase	σ_L expt. (10^{-21} cm^2)	σ_C expt. (10^{-23} cm^2)	σ_L DIRAC (10^{-21} cm^2)	σ_L LOSS (10^{-21} cm^2)	σ_C NRC+REC (10^{-23} cm^2)
CH_2	Gas	5.35±0.16	1.44±0.08	5.76	6.00	1.68
CH_2	Solid	6.91±0.20	1.46±0.07	6.47	6.32	1.68
C	Solid	6.87±0.21	1.21±0.06	5.76	5.75	1.31
N	Gas	6.56±0.20	1.63±0.08	6.75	7.13	1.60
Ne	Gas	12.70±0.38	2.71±0.15	12.8	13.8	3.91
Al	Solid	30.10±1.03	4.49±0.23	28.2	25.8	8.68
Ti	Solid	83.20±2.64	23.9±0.96	82.6	78.5	84.00

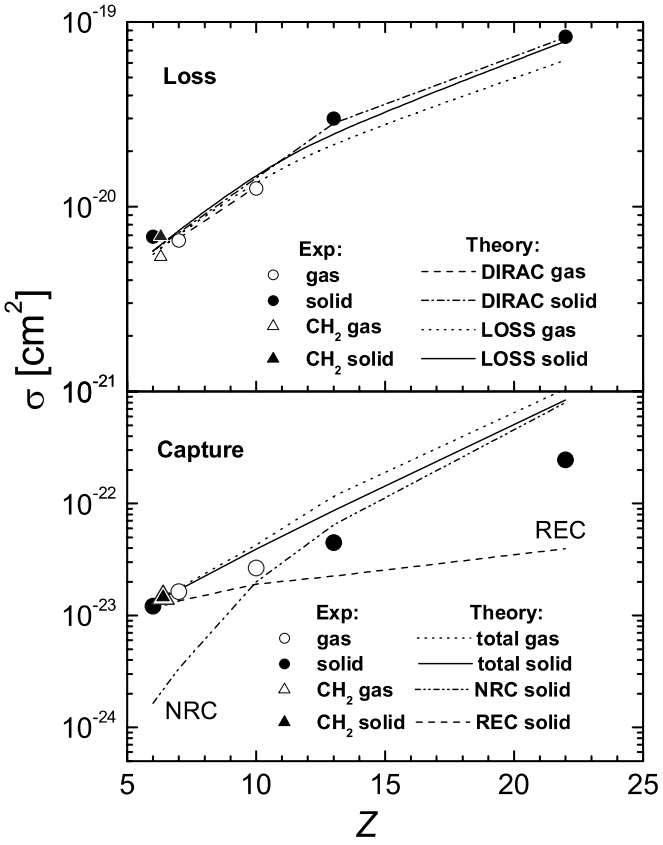

FIG. 2. Upper panel: Electron-loss cross sections for 200 MeV/u Ni^{27+} ions in gases and solids. The measured data are represented by symbols and the theoretical predictions [22,23] by lines; see legends. (See Fig. 3 for an expanded representation.) Lower panel: Electron-capture cross sections of 200 MeV/u bare Ni^{28+} ions in gas and solid targets. In both parts the measured data are represented by symbols and the theoretical predictions [22,25] by lines; see legends.

The experimental and theoretical electron-loss and electron-capture cross sections for gas and solid targets are given in Table I. All data are from the present study. The cross sections for the CH_2 group were determined from the polypropylene and ethylene data using Bragg's additivity rule.

In Fig. 2 the experimental and calculated cross sections are presented as a function of the target atomic number Z. The effective atomic numbers for the CH_2 compound of 6.3 and 6.4 were used for loss and capture, respectively. This follows from the Z^2+Z scaling for the ionization, and the Z^5 and Z scaling for the nonradiative (NRC) and radiative electron-capture (REC) processes, respectively. In the upper panel, the loss cross sections are compared with results from the DIRAC [22] and the LOSS [23] codes. Both theoretical models use a four-level scheme following the paper of Anholt [21]. The scheme includes electron capture, ionization, excitation, deexcitation, and radiative-decay processes of the bare and H-like Ni ions in the $1s$, $2s$, and $2p$ states. The influence of the $3s$, $3p$, and $3d$ levels of Ni^{27+} can be neglected at this collision energy. The $1s$ electron in H-like Ni ions can undergo a monopole excitation to the $2s$ state or a dipole excitation to the $2p$ state, while the $2s$ electron can be further excited into the $2p$ state. In addition to excitation, $2s$ and $2p$ states may also decay to lower levels by radiative decay, with probability amplitudes $A(2s\rightarrow 1s) \approx 4.64\times 10^9\ s^{-1}$ and $A(2p\rightarrow 1s)\approx 3.17\times 10^{14}\ s^{-1}$, or they can be depopulated by collisional deexcitation. The population dynamics of this four-state model is described by a system of rate equations which give the relative populations of the $1s$, $2s$, and $2p$ levels of H-like Ni ions as well as the fraction of bare ions and the loss and capture cross sections. Calculations with the DIRAC code apply the relativistic Dirac wave functions.

In addition, another theory was used to account for the target–density effects [24] by applying the LOSS [23] and CAPTURE [25] codes. The LOSS code calculates ionization and excitation cross sections by taking into account relativistic effects and the atomic structure of the target atom. The radial wave functions of atoms and ions are found by solving the Schrödinger equation in the effective field of the atomic core. The measured loss cross sections agree well with calculations applying both the DIRAC and LOSS codes (see Fig. 2).

The results for the electron-capture cross sections are shown in the lower panel of Fig. 2. The total capture cross section is presented as a sum of two contributions, the radiative and the nonradiative electron-capture processes. The REC cross sections were calculated by the DIRAC code [22] and the NRC cross sections by the CAPTURE code [25]. In the lower panel of Fig. 2, the measured capture cross sections are compared with theoretical predictions. For solid targets the contributions from REC and NRC are illustrated separately. The experimental electron-capture cross sections for the light target materials agree well with the theoretical predictions, whereas for high-Z targets the dominating NRC description has to be improved. The experimental capture cross sections for the light targets show no gas-solid effect as demonstrated for the CH_2 group. Only a very weak target-density dependence can be extracted for neighboring monatomic targets by a polynomial fit reflecting the theoretical Z dependence for REC and NRC processes. In this way a systematic enhancement of about $(5\pm 2)\%$ in gases is observed, which is qualitatively consistent with our theoretical prediction (see Fig. 2) and the Bohr-Lindhard model.

The situation for the loss cross sections is quite different. Already in Fig. 2 the experimental and theoretical results indicate a systematic difference for gases and solids. This observation is even more clearly demonstrated in Fig. 3, where the cross sections are scaled by the factor (Z^2+Z) for the different elements. The experimental and theoretical data clearly split into two well-separated groups, corresponding to solid and gaseous targets. It is observed that the measured ionization cross sections are about 40% higher in solids than in gases. Both theoretical predictions agree qualitatively with the experimental data, with the DIRAC code being slightly better.

In the present work, the loss and capture cross sections of 200 MeV/u bare and H-like Ni ions for gaseous and solid targets were measured. The selected energy lies in the intermediate energy range compared to the previous measurements carried out at 3.0 MeV/u for C ions [4] and 159.3 GeV/u for Pb ions [7], and has the advantage of focusing on simple well-defined and conclusive charge-

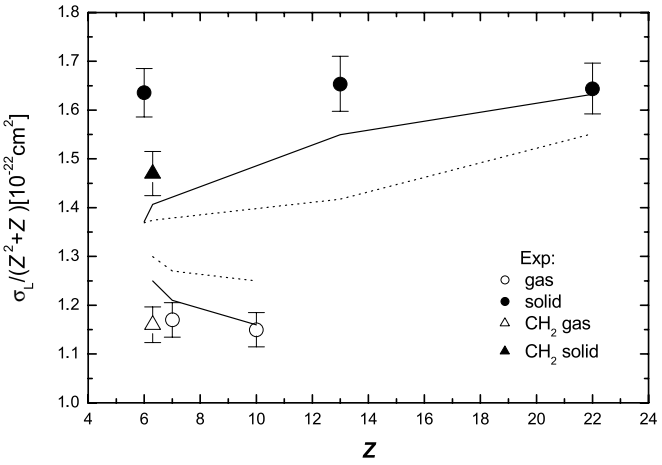

FIG. 3. Scaled experimental and theoretical electron-loss cross sections in gaseous and solid targets as a function of the target atomic number *Z*. Open symbols represent the gas data and full symbols the solid ones. The CH_2 compounds are indicated by triangles. The theoretical predictions from LOSS [23] and DIRAC codes [22] are indicated by dashed and solid lines, respectively.

changing conditions. Our experimental results agree well with recent theoretical developments taking the role of projectile excitation into account. A clear gas-solid difference in the electron-loss cross sections has been experimentally demonstrated. The measured data are in good agreement with both theories except for the capture cross sections in high-*Z* materials, thus revealing a challenge for future NRC theories. In principle, the gas-solid effect is expected to be even larger at lower velocities, but on the other hand, the more complex charge distribution and excited-state population would obscure the interpretation in simple microscopic terms.

In summary, our experimental results with relativistic heavy ions show that the Bohr-Lindhard model is the correct approach for the microscopic understanding of the experimental observations. Again, as in previous publications [26,27], this Rapid communication shows that with the new powerful accelerator and spectrometer facilities at relativistic energies, one can select specific experimental conditions which strongly reduce the complexity of ion interactions with matter and, thus, can give new insight into the basic understanding of heavy-ion interactions with matter.

It is a great pleasure to thank our technical staff, K.-H. Behr, A. Brünle, K.H. Burkhard, K. Dermati, and J. Steiner, for the excellent support in the preparation of the experimental setup and MEXT for financing H.O.'s stay at GSI. S.F. acknowledges support by the BMBF and GSI (Project No. KS-FRT).

[1] N. O. Lassen, K. Dan. Vidensk. Selsk. Mat. Fys. Medd. **26**, No. 5 (1951); **26**, No. 12 (1951).
[2] H. D. Betz, Rev. Mod. Phys. **44**, 465 (1972).
[3] H. Geissel, Y. Laichter, W. F. W. Schneider, and P. Armbruster, Nucl. Instrum. Methods Phys. Res. **194**, 21 (1982); Phys. Lett. **99A**, 77 (1983).
[4] C. J. Woods *et al.*, J. Phys. B **17**, 867 (1984).
[5] S. Della-Negra, Y. Le Beyec, B. Monart, K. Standing, and K. Wien, Phys. Rev. Lett. **58**, 17 (1987).
[6] R. Bimbot *et al.*, Nucl. Instrum. Methods Phys. Res. B **44**, 1 (1989).
[7] H. F. Krause *et al.*, Phys. Rev. A **63**, 032711 (2001).
[8] O. N. Rosmej *et al.*, Phys. Rev. A **72**, 052901 (2005).
[9] N. Bohr and J. Lindhard, K. Dan. Vidensk. Selsk. Mat. Fys. Medd. **28**, No. 7 (1954).
[10] H. D. Betz and L. Grodzins, Phys. Rev. Lett. **25**, 211 (1970).
[11] H. Geissel *et al.*, Nucl. Instrum. Methods Phys. Res. B **195**, 3 (2002).
[12] C. M. Frey *et al.*, Nucl. Instrum. Methods Phys. Res. B **107**, 31 (1996).
[13] D. I. Thwaites, Nucl. Instrum. Methods Phys. Res. B **69**, 53 (1992), and references therein.
[14] R. B. Baragiola *et al.*, J. Phys. B **9**, L447 (1979).
[15] H. D. Betz, R. Schramm, and W. Oswald, in *Interaction of Charged Particles with Solids and Surfaces*, NATO Advance Studies Institute, Series B: Physics, edited by A. Gras-Marti, H. M. Urbassek, N. R. Arista, and F. Flores (Plenum, New York, 1991), Vol. 271, p. 365.
[16] K. Blasche and B. Franczak, in *Proceedings of Third European Particle Accelerator Conference Berlin*, edited by H. Henke, H. Homeyer, and Ch. Petit-Jean-Genaz (Editions Fronitière, Gif-sur-Yvette, 1992), p. 9.
[17] H. Geissel *et al.*, Nucl. Instrum. Methods Phys. Res. B **204**, 71 (2003).
[18] M. Portillo *et al.*, Nucl. Instrum. Methods Phys. Res. B (to be published).
[19] H. Weick *et al.*, Nucl. Instrum. Methods Phys. Res. B **164**, 168 (2000).
[20] A. Närmann and P. Sigmund, Phys. Rev. A **49**, 4709 (1994).
[21] R. Anholt, Phys. Rev. A **31**, 3579 (1985).
[22] A. Surzhykov, S. Fritzsche, and P. Koval, Comput. Phys. Commun. **165**, 139 (2005).
[23] V. P. Shevelko *et al.*, Nucl. Instrum. Methods Phys. Res. B **184**, 295 (2001).
[24] V. P. Shevelko *et al.*, J. Phys. B **38**, 2675 (2005).
[25] V. P. Shevelko *et al.*, J. Phys. B **37**, 201 (2004).
[26] C. Scheidenberger *et al.*, Phys. Rev. Lett. **73**, 50 (1994); **77**, 3987 (1997).
[27] H. Weick *et al.*, Phys. Rev. Lett. **85**, 2725 (2000).